Inorganic Chemistry

Article

pubs.acs.org/IC

Broad Negative Thermal Expansion Operation-Temperature Window Achieved by Adjusting Fe−Fe Magnetic Exchange Coupling in La(Fe,Si)$_{13}$ Compounds

Shaopeng Li,[†,§] Rongjin Huang,[*,†] Yuqiang Zhao,[†,§] Wen Li,[†,§] Wei Wang,[†] Chuanjun Huang,[†] Pifu Gong,[‡,§] Zheshuai Lin,[‡] and Laifeng Li[*,†]

[†]State Key Laboratory of Technologies in Space Cryogenic Propellants, Technical Institute of Physics and Chemistry, Chinese Academy of Sciences, Beijing 100190, P.R. China

[‡]Beijing Center for Crystal R&D, Key Lab of Functional Crystals and Laser Technology, Technical Institute of Physics and Chemistry (TIPC), Chinese Academy of Sciences (CAS), Beijing 100190, P.R. China

[§]University of Chinese Academy of Sciences, Beijing 100049, P.R. China

Supporting Information

ABSTRACT: Cubic La(Fe,Si)$_{13}$-based compounds have been recently developed as promising negative thermal expansion(NTE) materials, but the narrow NTE operation-temperature window(~110 K) restricts their actual applications. In this work, we demonstrate that the NTE operation-temperature window of LaFe$_{13-x}$Si$_x$ can be significantly broadened by adjusting Fe−Fe magnetic exchange coupling as x ranges from 2.8 to 3.1. In particular, the NTE operation-temperature window of LaFe$_{10.1}$Si$_{2.9}$ is extended to 220 K. More attractively, the coefficients of thermal expansion of LaFe$_{10.0}$Si$_{3.0}$ and LaFe$_{9.9}$Si$_{3.1}$ are homogeneous in the NTE operation-temperature range of about 200 K, which is much valuable for the stability of fabricating devices. The further experimental characterizations combined with first-principles studies reveal that the tetragonal phase is gradually introduced into the cubic phase as the Si content increases, hence modifies the Fe−Fe interatomic distance. The reduction of the overall Fe−Fe magnetic exchange interactions contributes to the broadness of NTE operation-temperature window for LaFe$_{13-x}$Si$_x$.

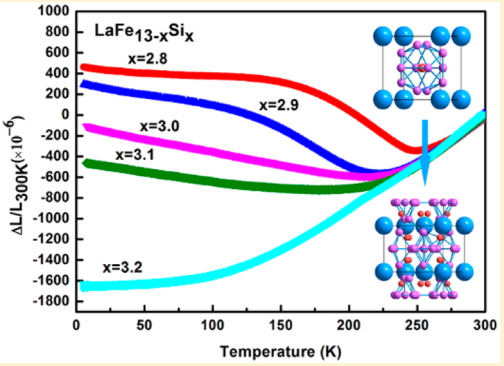

1. INTRODUCTION

Most materials expand when heated. This familiar phenomenon can be understood by accounting for the inherent anharmonicity of bond vibrations. A very limited number of materials, however, exhibit "abnormal" negative thermal expansion (NTE), that is, they expand when cooled instead of contracting. When mixed with common materials, they can form a composite with precisely tailored coefficient of thermal expansion (CTE). This is valuable in precision instruments such as space structures, electronic packaging, fiber optic systems and electro-optical sensor, in which it is necessary to compensate for the positive thermal expansion. Therefore, studies on NTE materials have been driven by a combination of fundamental interest in this relatively unusual property and the potential device applications.

Examples of the most studied NTE materials include several classes such as LiAlSiO$_4$(β-eucryptite), ZrW$_2$O$_8$,[1,2] ReO$_3$,[3] CuO nanoparticles,[4] materials family of ScF$_3$,[5−8] PbTiO$_3$-based compounds,[9] La(Fe,Si)$_{13}$-based compounds[10] and doped antiperovskite manganese nitride.[11−17] Among these NTE materials, the cubic La(Fe,Si)$_{13}$-based compounds are recently developed as promising NTE materials, which show large, isotropic and nonhysteretic NTE properties as well as relatively high electrical and thermal conductivity. It is noteworthy, however, that NTE occurs in only a narrow temperature range, generally less than 110 K as reported in earlier paper.[10] To promote an even wider range of practical applications, it is desired to develop new La(Fe,Si)$_{13}$-based compounds with broad NTE operation-temperature window.

According to analysis of lattice and magnetic properties in previous studies, the NTE property of La(Fe,Si)$_{13}$-based compounds originates from magnetovolume effect (MVE), wherein a large volume contraction is triggered by the break of magnetic order, i.e., magnetic transition from a low-temperature ferromagnetic (FM) phase to a high-temperature paramagnetic (PM) phase.[18] Moreover, the magnetic properties are correlated to crystal structure, especially the Fe−Fe interatomic distance that is closely associated with the strength of Fe−Fe magnetic exchange coupling. It was reported that the crystal structure of LaFe$_{13-x}$Si$_x$ compound is dependent on the Si content, which leads to a cubic structure with the space group $Fm3c$ to tetragonal structure with $I4/mcm$ transition from x = 1.4 to 5.0. With $1.4 \le x \le 2.6$, LaFe$_{13-x}$Si$_x$ forms the cubic

Received: April 22, 2015
Published: July 21, 2015

DOI: 10.1021/acs.inorgchem.5b00908
Inorg. Chem. 2015, 54, 7868−7872

structure with the space group $Fm3c$ and shows ferromagnetic (FM) at low temperature, and with $3.2 \leq x \leq 5.0$, it forms the tetragonal one with the space group $I4/mcm$[19] and shows paramagnetic character. The $LaFe_{13-x}Si_x$ compounds with tetragonal structure ($I4/mcm$) present weak Fe−Fe magnetic exchange interactions, if the $LaFe_{13-x}Si_x$ phase with tetragonal structure and that with cubic structure can form a quasi composite, the strength of overall Fe−Fe exchange coupling tend to decrease. Therefore, it needs less thermal energy to break the magnetic order, which may result in a low shift of the starting temperature of NTE. In addition, we deduce that the CTE of this quasi composite may also decrease compared with pure cubic $LaFe_{13-x}Si_x$ compounds because the positive thermal expansion of the tetragonal phase would to some extent counteracts the NTE behavior. According to previous reports, the $LaFe_{13-x}Si_x$ compounds undergo a cubic ($Fm3c$)-tetragonal ($I4/mcm$) transition when x increases from 2.6 to 3.2. Therefore, we fabricated $LaFe_{13-x}Si_x$ compounds with x ranging from 2.8 to 3.2, the NTE properties of which were also further investigated in present study. Intriguingly, we found that broad NTE operation-temperature window up to 200 K can be achieved in $LaFe_{13-x}Si_x$ materials ($2.9 \leq x \leq 3.1$).

2. EXPERIMENTAL INFORMATION

All measurements were carried out using polycrystalline samples. A series of $LaFe_{13-x}Si_x$ ($2.8 \leq x \leq 3.2$) compounds were prepared in an arc melting furnace under a high-purity argon atmosphere. The raw materials of Fe, Si, and La were at least 99.9% pure. An excess 10 at % of La over the stoichiometric composition was added to compensate for loss during melting. Button samples were melted four times, and each time during melting the buttons were turned over to ensure homogeneity. The arc-melted ingots wrapped by Ta foils were sealed in a quartz tube filled with high-purity argon gas, subsequently homogenized at 1050 °C for 30 days, and finally quenched quickly into cold water.

In situ powder X-ray diffraction (XRD) was employed to identify the phase constitutions and crystal structure at different temperatures. The ambient and variable temperature XRD data were collected on a BRUKER D8-discover diffractometer using Cu Kα radiation (λ = 1.5406 Å, operation voltage 40 kV, current 40 mA). The linear thermal expansion data ($\Delta L/L_{(300K)}$) ($\Delta L/L=\Delta V/3V$) were acquired by using a high-resolution strain gage over a temperature range of 4−300 K. The measurement of linear thermal expansion in this way requires a reference material with known thermal expansion coefficient (ZERODUR glass ceramic, whose coefficient of thermal expansion (CTE) is nearly zero). The magnetic properties were measured by means of a physical property measurement system (PPMS-14T, Quantum Design) equipped with AC Magnetometer System (ACMS) option.

3. RESULTS AND DISCUSSION

3.1. Thermal Expansion Properties. Figure 1 displays linear thermal expansion ($\Delta L/L$) data (reference temperature = 300 K) as a function of temperature for $LaFe_{13-x}Si_x$ (x = 2.8, 2.9, 3.0, 3.1, and 3.2) in the temperature range of 4−300 K. All the samples have a positive thermal expansion with similar variability in the temperature range of 270−300 K. In contrary, the $\Delta L/L$ is strikingly affected by Si content as temperature decreases from 250 to 100 K. It can be seen that for all samples, except for x = 3.2, there exists a temperature region in which the $\Delta L/L$ increases with decreasing temperature, that is, NTE occurs. As increasing Si content, the cutoff temperature of NTE moves toward lower temperature region. For example, the NTE in $LaFe_{10.2}Si_{2.8}$ occurs from 250 K, whereas the NTE of the $LaFe_{10.0}Si_{3.0}$ and the $LaFe_{9.9}Si_{3.1}$ takes place from 210 and 178

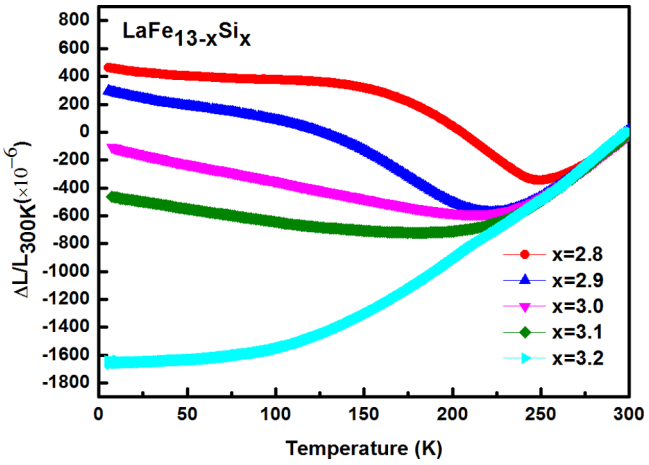

Figure 1. Temperature dependence of linear thermal expansions $\Delta L/L$ (reference temperature = 300 K) of $LaFe_{13-x}Si_x$ (x = 2.8, 2.9, 3.0, 3.1, and 3.2) in the temperature range of 4−300 K.

K, respectively. Moreover, it is noteworthy that the thermal expansion behavior under low temperature is strongly affected by partial substitution of Si for Fe. For instance, the $LaFe_{10.2}Si_{2.8}$ shows near zero thermal expansion behavior below the NTE temperature region, the average CTE, defined as $((\Delta L/L)_{T2} - (\Delta L/L)_{T1})/(T_2 - T_1)$, is -0.9×10^{-6} K^{-1} between 135 and 5 K (ΔT = 130 K). In contrast, the slopes α of the $LaFe_{13-x}Si_x$ (x = 2.9, 3.0, 3.1) are still negative even down to 4K. With further substitution of Si for Fe, the $LaFe_{9.8}Si_{3.2}$ exhibits positive thermal expansion behavior in the whole tested temperature region and the slope α grows gradually with increasing temperature.

Fascinatingly, the NTE operation-temperature windows of $LaFe_{13-x}Si_x$ are significantly broadened as the Si content varies from x = 2.9 to 3.1. For instance, the NTE operation-temperature window of the $LaFe_{9.9}Si_{3.1}$ and $LaFe_{10.0}Si_{3.0}$ are extended to 190 and 210 K, respectively. For $LaFe_{10.1}Si_{2.9}$, the NTE operation-temperature window reaches a considerably wide temperature range of 220 K, which is almost twice larger than that of the typical MVE-driving NTE materials, such as $La(Fe, Si, Co)_{13}$ compounds[10] and doped antiperovskite manganese nitrides.[11−17] Besides, the average CTE is -3.9×10^{-6} K^{-1} between 225 and 5 K (ΔT = 220 K) for $LaFe_{10.1}Si_{2.9}$. More interestingly, the $\Delta L/L$ curves show an almost linear increase with decrease in temperature for $LaFe_{10.0}Si_{3.0}$ and $LaFe_{9.9}Si_{3.1}$, which suggests the homogeneity of the coefficient of thermal expansion (CTE) in the NTE operation-temperature window. This feature is an unusual finding since the $\Delta L/L$ curves are in the sinusoidal shape in most literatures. Such broad negative thermal expansion operation-temperature window and outstanding homogeneity of the CTE suggest their more extensive potential applications. The average CTE are -2.5×10^{-6} K^{-1} between 214 and 4 K (ΔT = 210 K) and -1.4×10^{-6} K^{-1} between 194 and 4 K (ΔT = 190 K) for $LaFe_{10.0}Si_{3.0}$ and $LaFe_{9.9}Si_{3.1}$, respectively. On the basis of the special features, not only the implement of thermal expansion controlling and processing is much simpler, but also the ability and stability of NTE effect are improved.

3.2. Phase Composition and Crystal Structure. The powder X-ray diffraction measurement was carried out to identify the crystal structure and phase composition of the $LaFe_{13-x}Si_x$ samples. Figure 2a presents the XRD patterns of $LaFe_{13-x}Si_x$ (x = 2.8, 2.9, 3.0, 3.1, and 3.2) and the standard

DOI: 10.1021/acs.inorgchem.5b00908
Inorg. Chem. 2015, 54, 7868−7872

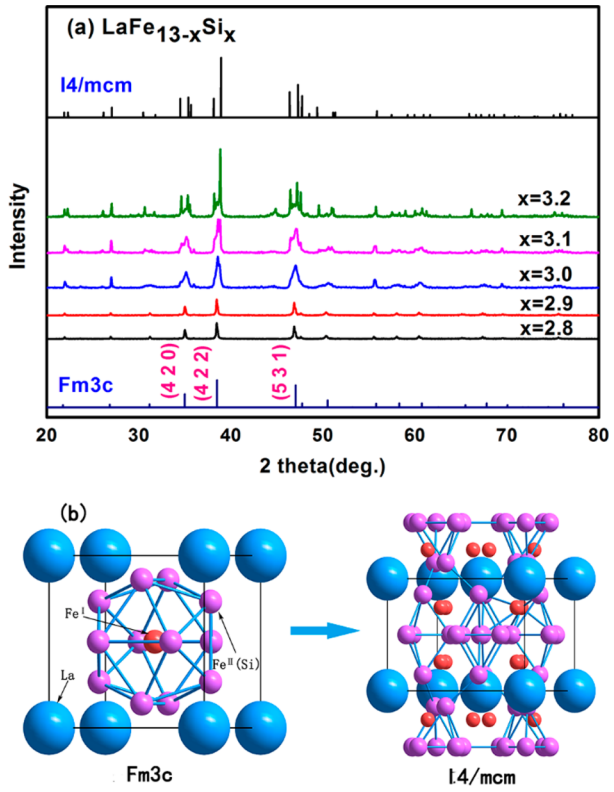

Figure 2. (a) X-ray diffraction patterns of $LaFe_{13-x}Si_x$ (x = 2.8, 2.9, 3.0, 3.1, and 3.2) and standard patterns with the space group *Fm3c* and *I4/mcm* at room temperature. (b) The schematic view of transition from cubic $NaZn_{13}$-type structure (space group *Fm3c*) to tetragonal derivative structure (space group *I4/mcm*) of $LaFe_{13-x}Si_x$ ($2.8 \leq x \leq 3.2$).

cards with the space group *Fm3c* and *I4/mcm* at room temperature. It indicates that all the samples have no visible diffraction peaks of pure elements or any other detectable phase in the patterns. Corresponding to the standard cards, we found that, by substituting Fe with a small amount of Si, it gradually undergoes a cubic (*Fm3c*)-tetragonal (*I4/mcm*) transition for $2.8 \leq x \leq 3.2$. The schematic view of transition from cubic structure to tetragonal derivative structure of $LaFe_{13-x}Si_x$ is displayed in Figure 2b. Specifically, the broad and relative weak reflection peaks (4 2 0), (4 2 2), and (5 3 1) of $LaFe_{13-x}Si_x$ with x = 2.8, 2.9 reflect that the main cubic structure coexist with minor tetragonal phase, while the three typical peaks of $LaFe_{13-x}Si_x$ with further substitution to x = 3.0, 3.1 become broader and begin to split, which is indicative of a cubic (*Fm3c*)-tetragonal (*I4/mcm*) phase transition. Finally, the diffraction peaks are in excellent agreement with the standard cards with the space group *I4/mcm* when x grows up to 3.2. Accordingly, we can certainly confirm that phase transition takes place in the samples of $LaFe_{13-x}Si_x$ when x ranges from 2.8 to 3.2. The tetragonal phase without NTE properties, as shown in Figure 1, although gradually reduces the absolute value of CTE in $LaFe_{13-x}Si_x$ compounds but gives rise to a valuable linear NTE properties and a broader NTE operation-temperature window.

The variable-temperature X-ray diffraction data for $LaFe_{13-x}Si_x$ compounds were also collected in order to study the structure of $LaFe_{13-x}Si_x$ at low temperatures where NTE behavior occurs. Figure 3a displays the representative pattern of $LaFe_{10.0}Si_{3.0}$ from 20 to 200 K. The characteristic reflection

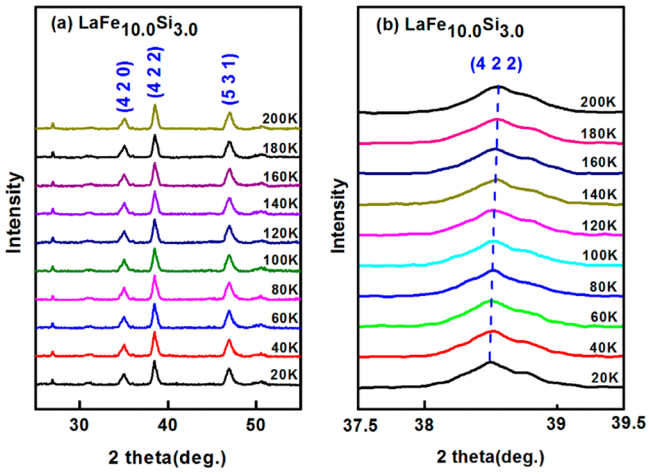

Figure 3. (a) X-ray diffraction peaks of (4 2 0), (4 2 2), and (5 3 1) for $LaFe_{10.0}Si_{3.0}$ at different temperatures. (b) Temperature dependence of (4 2 2) diffraction peak for $LaFe_{10.0}Si_{3.0}$ compound.

peaks of (4 2 0), (4 2 2), and (5 3 1) exist in the whole tested temperature range, which manifests that the $LaFe_{10.0}Si_{3.0}$ sample undergoes no structure transition when NTE occurs. However, the three reflection peaks move to lower 2θ angles with the decrease of temperature, which originates from the increase of lattice parameter according to the Bragg eq ($2d \sin \theta = n\lambda$). Therefore, we can conclude that the unit cell of $LaFe_{10.0}Si_{3.0}$ contracts as temperature increases from 20 to 200 K. For instance, it can be seen that, in the Figure 3b, the representative (4 2 2) reflection peak slightly shift to a lower angle. More intriguingly, the maximum of the (4 2 2) peak can be perfectly connected by a straight line, which reconfirms that, as previously stated in this paper, the homogeneity of the coefficient of thermal expansion in the NTE operation-temperature window.

3.3. Magnetic Properties. Considering that the NTE behavior in $LaFe_{13-x}Si_x$ is triggered by magnetic transition, an investigation of the magnetic properties would be very beneficial for elucidating the underlying mechanisms of the NTE properties. Figure 4a shows the temperature dependence of magnetization $M(T)$ for $LaFe_{13-x}Si_x$ (x = 2.8, 2.9, 3.0, and 3.1) measured at 0.01 T under zero-field-cooled (ZFC) process. Clearly, all the $M(T)$ curves exhibit an increase with decreasing temperature around the Curie temperature (T_c) corresponding to ferromagnetic−paramagnetic (FM−PM) phase transition. It is worth noting that the magnetic transition rate is affected by the Si content. The $M(T)$ curve of the $LaFe_{10.2}Si_{2.8}$ exhibits a sharp magnetic transition at 250 K, then remains constant with further decrease in temperature. As comparison, the $M(T)$ curves for $LaFe_{13-x}Si_x$ (x = 2.9, 3.0, 3.1) first increase rapidly and then more slowly as temperature decreases, which makes the FM−PM phase transition become a gradual process and further gives rise to a broad NTE operation-temperature window. The results coincide well with the temperature dependence of linear thermal expansion (shown in Figure 1), implying the close correlations between NTE behavior and magnetic transition.

It has been found that in some invar or invar-like compounds, for example, $Fe_{65}Ni_{35}$ and $YFe_{10}Mo_2$, the spontaneous magnetostriction $\omega_s(T)$ is approximately proportional to the square of the spontaneous magnetization $M_s^2(T)$ in temperature range of $0 < T < T_c$, namely, $\omega_s(T) = CM_s^2(T)$,

DOI: 10.1021/acs.inorgchem.5b00908
Inorg. Chem. 2015, 54, 7868−7872

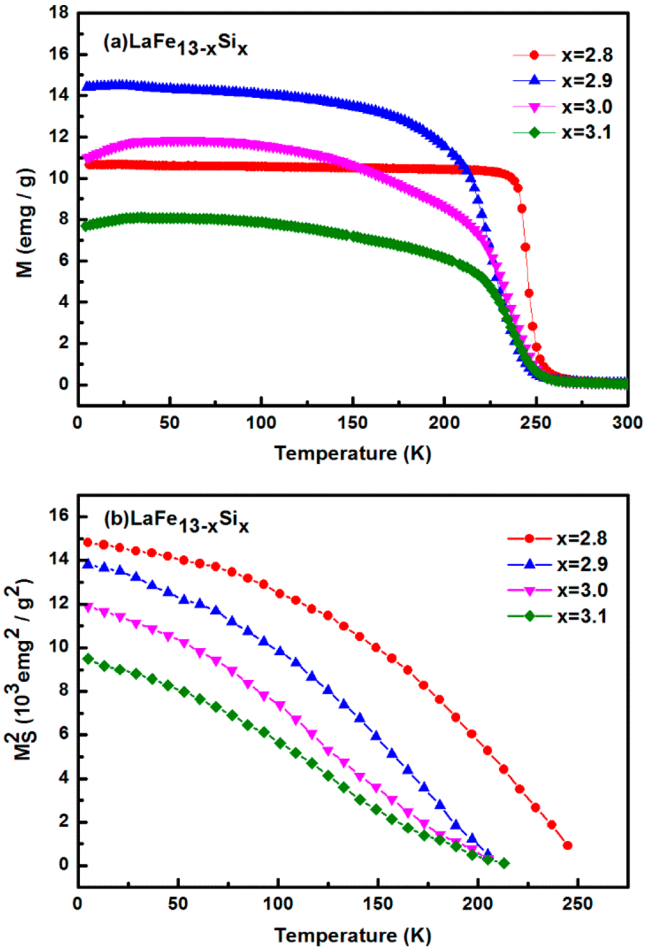

Figure 4. (a) Temperature dependence of magnetization $M(T)$ under zero-field-cooled process at 0.01 T for $LaFe_{13-x}Si_x$. (b) Square of the spontaneous magnetization as a function of the temperature $M_s^2(T)$ for $LaFe_{13-x}Si_x$ below the Curie temperature.

where C is the magnetoelastic coupling constant.[20] Therefore, the $M_s^2(T)$ curves can reflect the strength of spontaneous magnetostriction, which can bring about NTE behavior. The isothermal magnetization versus applied field $M(H)$ were measured at different temperatures to research the effect of Si doping on spontaneous magnetostriction, also to better clarify the mechanisms of NTE. The spontaneous magnetization $M_S(T)$ is deduced from the Arrott plots below T_c by extrapolating the Arrott plots to $H/M = 0$. Figure 4b displays temperature dependent $M_s^2(T)$ for all samples, the square of the spontaneous magnetization, that is, spontaneous magnetostriction, decreases with increasing Si content at the same temperature. Compared with the linear thermal expansion $(\Delta L/L)$ data, we find that higher $M_s^2(T)$ leads to larger values of $\Delta L/L$ at the same temperature. On the other hand, $M_s^2(T)$ increases with a decrease of the temperature for all the samples, but the rising rate is different from the others. By comparing Figure 1 with Figure 4b, one can clearly see that the rising rate of $\Delta L/L$ synchronizes with that of $M_s^2(T)$, relative larger rising rate of spontaneous magnetization for the $LaFe_{13-x}Si_x$ (x = 3.0 and 3.1) leads to an increase of $\Delta L/L$ with decreasing temperature at very low temperatures, contributing to stronger NTE behavior than $LaFe_{13-x}Si_x$ (x = 2.8 and 2.9) at very low temperatures. The above results prove that the variation of spontaneous magnetization, that is, spontaneous magnetostriction, affected by Si doping accounts for the different NTE behavior of $LaFe_{13-x}Si_x$ compounds.

3.4. Theoretical Calculation. In addition, the abnormal low-temperature shift of NTE operation-temperature window with Si content was discussed based on theoretical calculation. According to our previous reports of $LaFe_{13-x}Si_x$ (x = 1.5, 1.8, 2.1, 2.4), the NTE operation-temperature window shifts toward higher temperature region when the Si content increases from x = 1.5 to 2.4.[10,21] The Curie temperature(T_c) of $LaFe_{13-x}Si_x$ is in reasonable agreement with the NTE operation-temperature window, which is mostly determined by the strength of the Fe−Fe exchange coupling.[22] In the cubic structure (space group $Fm3c$) of $La(Fe,Si)_{13}$-based compounds, as depicted in the Figure 2b, Fe atoms occupy two nonequivalent sites, that is, 8b(Fe^I) and 96i(Fe^{II}), respectively. The Fe^I atom is surrounded by an icosahedron with 12 Fe^{II} atoms, and the Fe^{II} atom has 1 Fe^I atom and 9 Fe^{II} atoms as the nearest neighbors.[23] There exists two types of Fe−Fe exchange interactions in the cubic $LaFe_{13-x}Si_x$ compounds, previous studies reported that T_c of cubic $LaFe_{13-x}Si_x$ mainly affected by Fe^I−Fe^{II} exchange interactions.[24] The first-principles geometry optimization calculations for $LaFe_{13-x}Si_x$ ($2.8 \le x \le 3.1$) at 0 K are performed by using CASTEP package, as displayed in Table 1,

Table 1. Fe^I−Fe^{II} Interatomic Distance of $LaFe_{13-x}Si_x$ as a Function of Si Content

Si content	2.8	2.9	3.0	3.1
d (Å)	2.498	2.500	2.502	2.503

the Fe^I−Fe^{II} interatomic distances increase with Si content in the range of 2.8−3.1, which permits the Fe 3d band to narrow and strengthen the Fe^I−Fe^{II} magnetic exchange couplings by reducing the overlap of the Fe 3d wave functions. Hence, we infer that the introduction of the tetragonal phase weakens Fe^{II}−Fe^{II} magnetic exchange interactions, which may be responsible for the decrease of T_c and the low-temperature shift of NTE operation-temperature window. As clearly seen in Figure 4a, the $M(T)$ curves of $LaFe_{10.0}Si_{3.0}$ and $LaFe_{9.9}Si_{3.1}$ grows with temperature rise below 50K, which is a characteristic of the emergence of the antiferromagnetic phase from the ferromagnetic phase. It is well-known that the Fe−Fe magnetic exchange interactions of antiferromagnetic phase are weaker than that of ferromagnetic phase, thus we deduce that the antiferromagnetic phase induced by tetragonal phase probably bring about the abnormal shift of T_c. Further theoretical studies are necessary to address this issue more thoroughly.

4. CONCLUSIONS

In present work, the NTE operation-temperature window of $LaFe_{13-x}Si_x$ was effectively broadened with further increasing the amount of Si element from x = 2.9 to 3.1. Specifically, the NTE operation-temperature window of $LaFe_{10.1}Si_{2.9}$ can be extended to a wide temperature range of 220 K. More intriguingly, the CTE of $LaFe_{10.0}Si_{3.0}$ and $LaFe_{9.9}Si_{3.1}$ are homogeneous in their NTE operation-temperature range of about 200 K, which is much valuable for the stability of fabricating devices. Furthermore, the broadness of NTE operation-temperature window is attributed to the reduction of the overall Fe−Fe magnetic exchange couplings on the basis of theoretical calculation and magnetic properties measurement. Also, the phase coexistence and transition of cubic structure and tetragonal structure of $LaFe_{13-x}Si_x$ were

DOI: 10.1021/acs.inorgchem.5b00908
Inorg. Chem. 2015, 54, 7868−7872

confirmed by powder X-ray diffraction characterization. In brief, we have prepared $LaFe_{13-x}Si_x$ materials with broad NTE operation-temperature window in our study, which can promote them highly potential in diversely practical applications.

■ ASSOCIATED CONTENT

Supporting Information

The calculated method details of $Fe^{I}-Fe^{II}$ interatomic distance for $LaFe_{13-x}Si_x$ (x = 2.8, 2.9, 3.0, 3.1). The Supporting Information is available free of charge on the ACS Publications website at DOI: 10.1021/acs.inorgchem.5b00908.

■ AUTHOR INFORMATION

Corresponding Authors

*E-mail: huangrongjin@mail.ipc.ac.cn.
*E-mail: laifengli@mail.ipc.ac.cn.

Notes

The authors declare no competing financial interest.

■ ACKNOWLEDGMENTS

This work was supported by the National Natural Science Foundation of China (Nos. 51232004, 51377156, 51401224), the National Magnetic Confinement Fusion Science Program (Grant No. 2015GB121001), the fund of the State Key Laboratory of Technologies in Space Cryogenic Propellants, SKLTSCP1204, and the Special Foundation of the Director Technical Institute of Physics and Chemistry, CAS.

■ REFERENCES

(1) Mary, T. A.; Evans, J. S. O.; Vogt, T.; Sleight, A. W. *Science* **1996**, *272*, 90−92.
(2) Perottoni, C. A.; Jornada, J. A. H. *Science* **1998**, *280*, 886−889.
(3) Chatterji, T.; Hansen, T. C.; Brunelli, M.; Henry, P. F. *Appl. Phys. Lett.* **2009**, *94*, 241902−3.
(4) Zheng, X. G.; Kubozono, H.; Yamada, H.; Kato, K.; Ishiwata, Y.; Xu, C. N. *Nat. Nanotechnol.* **2008**, *3*, 724−726.
(5) Li, C. W.; Tang, X. L.; Muñoz, J. A.; Keith, J. B.; Tracy, S. J.; Abernathy, D. L.; Fultz, B. *Phys. Rev. Lett.* **2011**, *107*, 195504.
(6) Greve, B. K.; Martin, K. L.; Lee, P. L.; Chupas, P. J.; Chapman, K. W.; Wilkinson, A. P. *J. Am. Chem. Soc.* **2010**, *132*, 15496−15498.
(7) Morelock, C. R.; Gallington, L. C.; Wilkinson, A. P. *Chem. Mater.* **2014**, *26*, 1936−1940.
(8) Hu, L.; Chen, J.; Fan, L. L.; Ren, Y.; Rong, Y. C.; Pan, Z.; Deng, J. X.; Yu, R. B.; Xing, X. R. *J. Am. Chem. Soc.* **2014**, *136*, 13566−13569.
(9) Chen, J.; Nittala, K.; Forrester, J. S.; Jones, J. L.; Deng, J. X.; Yu, R. B.; Xing, X. R. *J. Am. Chem. Soc.* **2011**, *133*, 11114−11117.
(10) Huang, R. J.; Liu, Y. Y.; Fan, W.; Tan, J.; Xiao, F. R.; Qian, L. H.; Li, L. F. *J. Am. Chem. Soc.* **2013**, *135*, 11469−11472.
(11) Takenaka, K.; Takagi, H. *Appl. Phys. Lett.* **2005**, *87*, 261902.
(12) Sun, Y.; Wang, C.; Wen, Y. C.; Zhu, K. G.; Zhao, J. T. *Appl. Phys. Lett.* **2007**, *91*, 231913.
(13) Sun, Y.; Wang, C.; Huang, Q. Z.; Guo, Y. F.; Chu, L. H.; Arai, M.; Yamaura, K. *Inorg. Chem.* **2012**, *51*, 7232−7236.
(14) Song, X. Y.; Sun, Z. H.; Huang, Q. Z.; Rettenmayr, M.; Liu, X. M.; Seyring, M.; Li, G. N.; Rao, G. H.; Yin, F. X. *Adv. Mater.* **2011**, *23*, 4690−4694.
(15) Qu, B. Y.; Pan, B. C. *J. Appl. Phys.* **2010**, *108*, 113920.
(16) Lin, J. C.; Wang, B. S.; Lin, S.; Tong, P.; Lu, W. J.; Zhang, L.; Song, W. H.; Sun, Y. P. *J. Appl. Phys.* **2012**, *111*, 043905.
(17) Tong, P.; Louca, D.; King, G.; Llobet, A.; Lin, J. C.; Sun, Y. P. *Appl. Phys. Lett.* **2013**, *102*, 041908.
(18) Hu, F. X.; Shen, B. G.; Sun, J. R.; Cheng, Z. H.; Rao, G. H.; Zhang, X. X. *Appl. Phys. Lett.* **2001**, *78*, 3675−3677.
(19) Chang, H.; Chen, N.; Liang, J.; Rao, G. *J. Phys.: Condens. Matter* **2003**, *15*, 109.
(20) Podgornykh, S. M.; Kazantsev, V. A. *Phys. Met. Metallogr.* **2010**, *109*, 247.
(21) Wang, W.; Huang, R. J.; Li, W.; Tan, J.; Zhao, Y. Q.; Li, S. P.; Huang, C. J.; Li, L. F. *Phys. Chem. Chem. Phys.* **2015**, *17*, 2352.
(22) Han, M.; Miller, G. *Inorg. Chem.* **2008**, *47*, 515.
(23) Wang, G.; Wang, F.; Di, N. L.; Shen, B.; Cheng, Z. *J. Magn. Magn. Mater.* **2006**, *303*, 84.
(24) Bo, L. X.; Altounian, Z.; Ryan, D. H. *J. Phys.: Condens. Matter* **2003**, *15*, 7385−7394.

DOI: 10.1021/acs.inorgchem.5b00908
Inorg. Chem. 2015, 54, 7868−7872